Extreme Mechanics Letters 23 (2018) 9–16

Contents lists available at ScienceDirect

Extreme Mechanics Letters

journal homepage: www.elsevier.com/locate/eml

The effect of surface bending and surface stress on the transmission of a vertical line force in soft materials

Chung-Yuen Hui [a,*], Zezhou Liu [a], Anand Jagota [b]

[a] Department of Mechanical and Aerospace Engineering, Field of Theoretical and Applied Mechanics, Cornell University, Ithaca, NY 14853, USA
[b] Departments of Bioengineering and of Chemical & Biomolecular Engineering, 111 Research Drive, Lehigh University, Bethlehem, PA 18015, USA

ARTICLE INFO

Article history:
Received 11 May 2018
Received in revised form 5 July 2018
Accepted 13 July 2018
Available online 23 July 2018

Keywords:
Surface bending
Surface stress
Elasto-capillary length
Elasto-bending length

ABSTRACT

When the surface of a soft substrate that carries a constant in-plane residual stress is indented by a concentrated line force, its profile near the applied load is found to have a kink, which results from a local balance of the surface stresses and the imposed force. Although the local bulk stresses in the substrate no longer have a net contribution to this force balance, they nevertheless grow according to a weak logarithmic singularity with respect to distance from the line load. Here we study how a normal line load is transmitted across a solid surface that can provide additional resistance due to bending deformation; we present an exact closed-form solution. Our analysis shows that the ability of the surface to resist bending completely regularizes the stress field — it is continuously differentiable everywhere. In particular, the stress state in the elastic substrate is hydrostatic right underneath the line load if the material is incompressible. Its maximum value is directly proportional to the applied normal load and inversely proportional to the elasto-bending length. It also depends on a dimensionless parameter which is the ratio of the elasto-capillary length to the elasto-bending length.

1. Introduction

Several studies over the past decade [1–3] have established the important and often dominant role of the surface of soft solids in their mechanical response. By far, the most commonly studied case is one in which the surface carries a constant and isotropic in-plane residual stress. Models for many canonical phenomena involving forces applied to surfaces of soft solids, such as the wetting by a liquid drop [4,5], and indentation of soft elastic substrates [6–8] have been re-examined and found to be qualitatively altered. Much less attention has been paid to more complex surface properties such as surface elasticity (strain-dependent resistance to stretching) and surface bending (resistance to surface curvature), although these have both been proposed theoretically [9–13] and are clearly present in some systems [14,15]. A fundamental problem that forms the basis for analysis of more complex phenomena is the response of a surface to a line load. In this work we study how a surface that, in addition to an in-plane stress carries bending energy, affects the transmission of a line force acting on it.

In wetting, the vertical component of a droplet's surface tension (locally a line load) pulls the surface of the soft substrate upwards, leading to the formation of a ridge at and near the applied line load [5,16]. When the role of the surface is negligible, a classical result of the theory of elasticity predicts that the local displacement under a line load has a logarithmic singularity, which results in a local stress field with a $1/r$ singularity, where r is the distance from the line load [17]. That is, within this theory, the displacement under the applied load diverges logarithmically with distance from it. However, for single-phase soft materials that carry a constant surface stress and have no bending resistance, if the elasto-capillary length is larger than molecular dimensions, experiments and theory [5,16,18,19] show that the local ridge geometry is a kink with finite displacement. The local angles of the lines that meet at the kink are described by balance of surface stresses at the contact line –Neumann's triangle of forces – where the surface stresses of the solid balance the force exerted by the contact line. This local picture is shown in Fig. 1 for the special case where the entire surface has the same isotropic surface stress or surface tension,σ. Hence, locally, the line force N is usually transmitted fully to the surfaces, and theory predicts that the displacements are bounded and the stresses have a weak logarithmic singularity.

The line load problem has been studied theoretically by several research groups [1,19–22]. These studies assumed: (1) small deformation based on linearized theory of elasticity, (2) the surface can be treated as a membrane with *isotropic surface stress* $\sigma \boldsymbol{I}_s$, where $\boldsymbol{I}_s$ the isotropic surface tensor and σ is the magnitude of (tensile) surface stress (often called *surface tension*) which is assumed to be independent of the surface stretch. More relevant to this work, the

* Correspondence to: 322 Kimball Hall, Cornell University, Ithaca, NY 14853, USA.
E-mail address: ch45@cornell.edu (C.-Y. Hui).

https://doi.org/10.1016/j.eml.2018.07.003
2352-4316/

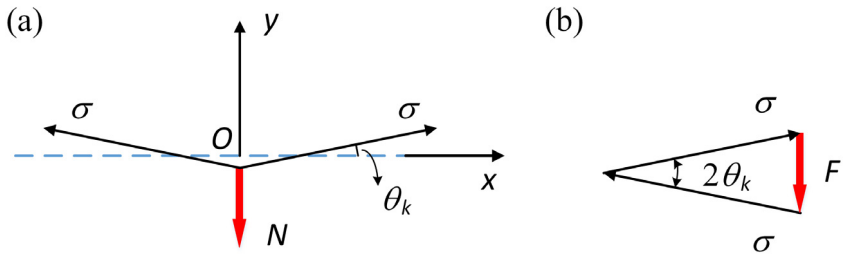

Fig. 1. Balance of forces at the kink formed on a soft solid when a line load is applied to it. The soft solid occupies the half space below the dashed blue line in (a). (a) Local geometry of kink. The deformed surface has a kink right underneath the line load. The vertical component of the surface tension, N, balances the applied force. (b) Local force balance requires that the surface stress σ and the applied line force N form a closed triangle, which is commonly known as the Neumann triangle.

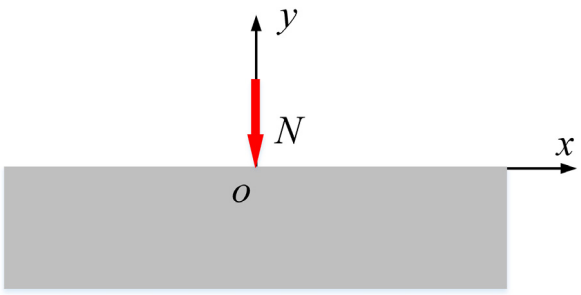

Fig. 2. Schematic of loading geometry. The elastic body occupies the lower half space y <0. A compressive line load of magnitude N >0 is imposed at the origin. N has units of force per unit length.

surface is assumed to have no bending rigidity. Here we note that most of the experimental studies of elasto-capillary phenomenon have focused on hydrogels where these assumptions are reasonable. Gurtin and Ian Murdoch [9] have raised the possibility that surfaces of elastic solids can store energy in bending but this issue has not received much attention. The exception is the work by Steigmann and Ogden [11] who develop constitutive models for surface with bending resistance. There are several examples of soft interfaces that can support both bending and tension. An example which is relevant to biology is the lipid bilayer where resistance to stretching is high, deformations of the bilayer generally conserve area, and the strain energy density of the interface is dominated by bending [13,23]. Kusumaatmaja et al. [15] have shown that the mechanics of the contact line between lipid bilayer membranes is governed by both surface bending and stress. A second example is where a new phase separates a soft solid from the air — e.g., a silica film a few nm thick that forms on the surface of an elastomer (e.g., polydimethylsiloxane) exposed to UV ozone or oxygen plasma [24,25]. These examples motivate us to study how an elastic substrate with surface bending and stress alters the transmission of force.

The plan of the paper is as follows. Section 2 states and formulates the problem. The exact solution is presented and results are discussed in Section 3. Section 4 concludes with a short summary.

2. Problem statement and formulation

The geometry is shown in Fig. 2 where an infinite block of a linear-elastic solid occupies the lower half space $|x| < \infty, y < 0$. The elasticity of the block is specified by its shear modulus μ and Poisson's ratio ν. Instead of a line load, we consider the more general situation where the surface at $y = 0$ is subjected to a *pressure load* $p_A(x)$, with no applied shear traction. This applied pressure is independent of the coordinate out of the plane of this page, i.e., perpendicular to x and y axis in Fig. 2 and we assume plane strain deformation where the out-of-plane displacement vanishes and the in-plane horizontal and vertical displacements u_1, u_2 are functions of the in-plane coordinates x and y only. We denote the in-plane stress and strain tensors in the elastic half space by $\sigma_{\alpha\beta}, \varepsilon_{\alpha\beta}$ respectively, where $\alpha, \beta = 1,2$.

In contrast to classical elasticity, the surface of the half space can resist deformation by bending and stretching. The bending stiffness of the surface is denoted by D. Stretching of the surface is resisted by surface tension σ, which we assume to be constant independent of surface stretch, as in previous works [7]. The change in curvature of the surface due to bending and stretching leads to a pressure *jump* of $-p_A(x) - \sigma_{22}\left(x, y = 0^-\right)$ across the interface. Here we use the standard convention that pressure is *negative* when tensile. This pressure jump is resisted by bending and stretching of the surface, and a simple force balance leads to

$$-p_A(x) - \sigma_{22}\left(x, y = 0^-\right) = D\frac{d^4u_2(x, y_2 = 0)}{dx^4} - \sigma\frac{d^2u_2(x, y = 0)}{dx^2}, \quad |x| < \infty \quad (1)$$

The first term on the RHS of (1) represents the pressure supported by bending, whereas the second term accounts for the curvature induced Laplace pressure due to surface tension. Thus, the behavior is governed by three materials parameters: D, σ, and μ. Absent the surface properties, D and σ, the problem of a response to a line force has no length scale associated with it in the sense that displacements and strains are everywhere proportional to the ratio N/μ. The introduction of the two surface properties, both of which are based on changes in surface shape, introduces two corresponding length scales that define distances over which the nature of the solution is altered. The characteristic distance over which bending alters the standard elasticity solution is given by $l_b = (\beta D/2\mu)^{1/3}$, where we call l_b the elasto-bending length. Here, $\beta \equiv 2(1-\nu)$, is introduced into this definition for later convenience. (For the common special case of an incompressible soft solid, $\beta = 1$.) We also define an elasto-capillary length $l_c = \beta\sigma/2\mu$, which defines a characteristic distance over which surface stress alters the elasticity solution. Thus, far from the line load, one expects standard elasticity always dominates (for a sufficiently large body.) Potentially, there are two other regions, one close to the line load where bending dominates and a second transition region at distances larger than l_b but less than l_c where surface stress dominates. Of course, whether the intermediate region exists is governed by the dimensionless ratio $\kappa \equiv l_c/l_b$, which needs to be significantly larger than unity for the existence of a region where surface stress dominates. It is evident that previous theories [7], which ignore bending, can be obtained by setting $D = 0$ in (1). Our definition of κ is similar in spirit to the parameter used by Charlotte et al. [26] and Paulsen et al. [27] (in our notation their parameter is $\sqrt{D/\sigma}$) who consider capillary wrapping of thin elastic sheets. Specifically, when κ is small, bending dominates and the effect of surface stress is not important. On the other hand, for large κ, bending dominates in a very small region underneath the line load, outside this region, surface stress dominates.

3. Method of solution

Using a formulation due to Marguerre [28], the displacements in the elastic body are determined by a stream function ϕ , i.e.,

$$u_1 = -\phi_{,12} \tag{2a}$$

$$u_2 = 2(1-\nu)\phi_{,11} + (1-2\nu)\,\phi_{,22} \tag{2b}$$

where a comma denotes partial derivative (e.g. $\partial\phi/\partial x \equiv \phi_{,1}$). The stream function satisfies the biharmonic equation

$$\nabla^4\phi = 0 \tag{3}$$

The stresses are obtained using the displacement field (2a, b) and the generalized Hooke's law. In terms of the stream function given by (2a, b), they are:

$$\sigma_{11} = 2\mu\,(1-\nu)\left[-\phi_{,112} + \frac{\nu}{1-\nu}\phi_{,222}\right] \tag{4a}$$

$$\sigma_{12} = 2\mu\,(1-\nu)\left[\phi_{,111} - \frac{\nu}{1-\nu}\phi_{,122}\right] \tag{4b}$$

$$\sigma_{22} = 2\mu\,(1-\nu)\left[\frac{2-\nu}{1-\nu}\phi_{,112} + \phi_{,222}\right] \tag{4c}$$

We define the Fourier transform (FT) of a function f by

$$\widetilde{f}\,(\lambda) \equiv \frac{1}{\sqrt{2\pi}}\int_{-\infty}^{\infty} f\,(x)\,e^{i\lambda x}dx \tag{5}$$

where λ is the transform variable. FT of (3) with respect to x results in an ODE for $\widetilde{\varphi}$ in y:

$$\lambda^4\widetilde{\varphi} - 2\lambda^2\widetilde{\varphi}_{yy} + \widetilde{\varphi}_{yyyy} = 0 \tag{6a}$$

The bounded solution of (6a) is

$$\widetilde{\varphi} = (A + By)\,e^{|\lambda|y}, \quad y < 0 \tag{6b}$$

where A *and* B are functions of λ to be determined by boundary conditions. We calculate the surface shear traction using (6b) in (4b). Setting this shear traction to zero on the surface then leads to the following relation between A and B,

$$-A\,|\lambda| = 2B\nu. \tag{7}$$

Using (2a, b), (6b) and (7), the *FT* of the displacements and stresses can be expressed in terms of B:

$$\widetilde{u}_1 = i\lambda\widetilde{\phi}_{,2} = i\lambda B\,[(1-2\nu) + |\lambda|\,y]\,e^{|\lambda|y} \tag{8a}$$

$$\widetilde{u}_2 = B\,|\lambda|\,e^{|\lambda|y}\,[2(1-\nu) - |\lambda|\,y] \tag{8b}$$

$$\widetilde{\sigma}_{11} = 2\mu e^{|\lambda|y}B|\lambda|^2\,[1 + |\lambda|\,y] \tag{8c}$$

$$\widetilde{\sigma}_{12} = 2\mu\,(i\lambda)\,|\lambda|^2 B y e^{|\lambda|y} \tag{8d}$$

$$\widetilde{\sigma}_{22} = 2\mu B|\lambda|^2 e^{|\lambda|y}\,[1 - |\lambda|\,y] \tag{8e}$$

The coefficient B is obtained by imposing the pressure jump condition (1) (after taking its *FT*). Using (8b), (8e) and (7); it is:

$$-\widetilde{p}_A\,(\lambda) - 2\mu B|\lambda|^2 = \left(D\lambda^4 + \sigma\lambda^2\right)2B\,|\lambda|\,(1-\nu)$$
$$\Rightarrow B = \frac{-\widetilde{p}_A\,(\lambda)\,/2}{\left(D\lambda^4 + \sigma\lambda^2\right)|\lambda|\,(1-\nu) + \mu|\lambda|^2}. \tag{9}$$

For the case of an applied line load,

$$p_A(x) = N\delta\,(x) \Rightarrow \widetilde{p}_A(\lambda) = \frac{N}{\sqrt{2\pi}} \tag{10}$$

where N is the magnitude of the line load (line load is *compressive* if $N > 0$)

As is well known, the displacement field of an infinitely extended elastic body due to a line load is not well defined, since at infinity it diverges logarithmically [17]. Mathematically, this behavior is reflected by $\widetilde{u}_\alpha$ having a non-integrable singularity of order $1/|\lambda|$ at $\lambda = 0$. This difficulty is avoided by computing the displacement gradient $u_{1,1}$ and $u_{2,1}$ since their FTs are well defined and are

$$-i\lambda\widetilde{u}_1 = \lambda^2 B e^{|\lambda|y}\,[(1-2\nu) + |\lambda|\,y] \tag{11a}$$

$$-i\lambda\widetilde{u}_2 = -i\lambda B\,|\lambda|\,e^{|\lambda|y}\,[2(1-\nu) - |\lambda|\,y]\,. \tag{11b}$$

3.1. Normalization

To expedite the analysis, we normalize all distances as $(X, Y) = (x, y)\,/l_b$ Displacements are normalized by N/μ and stresses by N/l_b. The normalized displacements are $U_\alpha = \mu u_\alpha/N$ and normalized stresses are $\Sigma_{\alpha\beta} = l_b\sigma_{\alpha\beta}/N$. In the following, we made use of the parity of the stresses and displacement fields; that is $\sigma_{11}, \sigma_{22}, u_2$ are even and σ_{12}, u_1 are odd functions of X respectively. Hence, we can limit our discussion to $X \geq 0$.

Using the parity of the displacement and stress fields, the normalized displacement gradients $U_{\alpha,1}$ and stresses $\Sigma_{\alpha\beta}$ for $X > 0$ can be found by finding the inverse FT of (8a)–(8e). In the appendix, we show that these fields can be expressed in terms of two dimensionless functions $I_1\,(X, Y)$ and $I_2\,(X, Y)$:

$$I_1\,(X, Y) \equiv \frac{1}{2\pi}\int_0^\infty C\,(\Lambda)\,e^{\Lambda Y}\cos\,(\Lambda X)\,d\Lambda \tag{12a}$$

$$I_2\,(X, Y) \equiv \frac{1}{2\pi}\int_0^\infty C\,(\Lambda)\,e^{\Lambda Y}\sin\,(\Lambda X)\,d\Lambda \tag{12b}$$

where

$$C\,(\Lambda) = \frac{1}{\Lambda^3 + \kappa\Lambda + 1}. \tag{12c}$$

In terms of these functions, the normalized displacements and stresses are (see the appendix):

$$\frac{\partial U_2}{\partial X} = \beta I_2 - Y\frac{\partial I_2}{\partial Y} \quad \beta \equiv 2(1-\nu) \tag{13a}$$

$$\frac{\partial U_1}{\partial X} = -\left[(1-2\nu)\,I_1 + Y\frac{\partial I_1}{\partial Y}\right] \tag{13b}$$

$$\Sigma_{11} = -2I_1 - 2Y\frac{\partial I_1}{\partial Y} \tag{13c}$$

$$\Sigma_{22} = -2I_1 + 2Y\frac{\partial I_1}{\partial Y} \tag{13d}$$

$$\Sigma_{12} = 2Y\frac{\partial I_1}{\partial X} \tag{13e}$$

Note that the normalized stresses given by (13c–e) do not explicitly depend on Poisson's ratio ν. The effect of Poisson's ratio is to rescale the stresses. In particular, if the material is incompressible, $\beta = 1$.

Eqs. (13c–e) imply that on the surface $Y = 0$, $\Sigma_{11} = \Sigma_{22}$ are principal stresses. In particular, if the material is incompressible, $\Sigma_{33} = (\Sigma_{22} + \Sigma_{11})\,/2$, then the material just under the surface is everywhere in a *state of hydrostatic tension/compression*.

We combine I_1 and I_2 by defining the complex function:

$$I(Z) \equiv I_1 + iI_2 = \frac{1}{2\pi}\int_0^\infty C(\Lambda)\, e^{i\Lambda Z} d\Lambda, \quad Z \equiv X - iY \tag{14}$$

Note $I_1 = \mathrm{Re}\, I$, $I_2 = \mathrm{Im}\, I_2$ and $Y \le 0$. In the appendix we will show that

$$I = \frac{1}{2\pi}\sum_{k=1}^{3} A_k e^{i\Lambda_k Z} E_1(i\Lambda_k Z) + 2\pi i e^{i\Lambda_2 Z}, \quad X > 0 \tag{15}$$

where E_1 is the exponential integral function [29] and Λ_j are the roots of the polynomial $\Lambda^3 + \kappa\Lambda + 1$, i.e.,

$$\Lambda_1 = \left[\sqrt{\frac{1}{4}+\frac{\kappa^3}{27}} - \frac{1}{2}\right]^{1/3} - \left[\sqrt{\frac{1}{4}+\frac{\kappa^3}{27}} + \frac{1}{2}\right]^{1/3} < 0 \tag{16a}$$

$$\Lambda_2 = -\frac{\Lambda_1}{2} + i\frac{\sqrt{3}}{2}\left\{\left[\sqrt{\frac{1}{4}+\frac{\kappa^3}{27}} - \frac{1}{2}\right]^{1/3} + \left[\sqrt{\frac{1}{4}+\frac{\kappa^3}{27}} + \frac{1}{2}\right]^{1/3}\right\} \tag{16b}$$

$$\Lambda_3 = \overline{\Lambda}_2 \tag{16c}$$

where a bar denotes complex conjugation. Thus, the first root lies on the negative real Λ axis and the other roots are complex conjugate of each other in the right half Λ plane. The special case where surface tension can be neglected in comparison with bending corresponds to $\kappa = 0$; for this case, the roots are $-1, e^{i\pi/3}, e^{-i\pi/3}$ respectively. The coefficients in (15) are:

$$A_1 = \frac{1}{(\Lambda_1-\Lambda_2)(\Lambda_1-\Lambda_3)},$$
$$A_2 = \frac{1}{(\Lambda_2-\Lambda_1)(\Lambda_2-\Lambda_3)}, A_3 = \overline{A}_2 \tag{17a}$$

Simple algebra shows that A_1 is real while A_2 and A_3 are complex conjugate of each other. Further,

$$A_1 + A_2 + A_3 = 0 \tag{17b}$$

3.2. Asymptotics and surface displacement gradient

In order to extract some physical understanding of what bending response, the principal new feature studied here, does to the nature of the deformation response, we examine the local surface displacement gradient near the line load, at $X = Y = 0$. While one can obtain the full description of the fields near the origin using the exact solution given by (13) and (15), a much simpler approach is to note that the normalized vertical surface displacement gradient (13a) is a *continuously differentiable function with zero slope* at the origin, indeed,

$$\frac{dU_2(X=0,Y=0)}{dX} = \beta I_2(X=0,Y=0) = \frac{\beta}{2\pi}\int_0^\infty \frac{\sin(\Lambda X)}{(\Lambda^3+\kappa\Lambda)+1} d\Lambda = 0 \tag{18}$$

This behavior is completely different from the classical elasticity solution where the *gradient* of the surface vertical displacement field at the origin *has a 1/x singularity*. Since the integrand of I_2 is differentiable for all $\Lambda \in [0,\infty)$ and decays to infinity as Λ^{-3}, we can differentiate I_2 with respect to X and its value at $X = 0$ is

$$I_2'(X=0,Y=0) = \frac{1}{2\pi}\left(\int_0^\infty \frac{\Lambda\cos\Lambda X}{(\Lambda^3+\kappa\Lambda)+1} d\Lambda\right)\Bigg|_{X=0} = \frac{1}{2\pi}\int_0^\infty \frac{\Lambda}{(\Lambda^3+\kappa\Lambda)+1} d\Lambda \tag{19}$$

However, the *second* derivative of $I_2(X, Y = 0)$ is *discontinuous* as $X \to 0^+$. To see this, we differentiate inside the integral sign to obtain

$$U_2'''(X,Y=0) = \beta I_2''(X,Y=0) = \frac{\beta}{2\pi}\int_0^\infty \frac{(\kappa\Lambda+2)\sin(\Lambda X)}{\Lambda(\Lambda^3+\kappa\Lambda+2)} d\Lambda - \frac{\beta}{2\pi}\int_0^\infty \frac{\sin(\Lambda X)}{\Lambda} d\Lambda \tag{20}$$

The first integral is a continuously differentiable function while the second integral is the Heaviside function. Hence $U_2''''(X)$ does not exist in the classical sense - it behaves as a delta function at the origin. Physically, the third derivative of the normal displacement must be discontinuous at the origin since the shear force due to bending there is responsible for resisting the applied line force.

The introduction of surface stress, as mentioned in the introduction, changes the divergent local displacement field of the purely elastic solution to one that has a kink in the surface shape. That is, the vertical displacement gradient in the absence of surface bending ($\kappa = \infty$) has a jump at the origin which gives rise to Neumann triangle of force balance. The addition of surface bending causes a continuous differentiable second derivative $U_2''(X) = \beta I_2'(X)$ or curvature at the origin, indicating that surface bending further regularizes the displacement, making its profile smooth.

The *full* description of the normal surface displacement gradient at the origin can be obtained from (15) using properties of the exponential integral function. The key is to evaluate I and study its behavior at the origin. For the surface normal displacement, we study the local behavior of I as $X \to 0^+, Y = 0$ (recognizing $\partial U_2/\partial X$ is odd). Using the series expansion of the exponential integral in (15), i.e.,

$$E_1(i\Lambda_k X) = \underbrace{-\gamma - \sum_{n=1}^{\infty}\frac{(-1)^n (i\Lambda_k X)^n}{nn!}}_{\chi(i\Lambda_k X)} - \ln(i\Lambda_k X), \quad |\mathrm{Arg}(i\Lambda_k)| < \pi \tag{21a}$$

where γ is the Euler constant. Substituting (21a) into (15) gives

$$I(X) = I_1 + iI_2 = \frac{1}{2\pi}\left\{-\Phi(X) + \sum_{k=1}^{3} A_k e^{i\Lambda_k X}\chi(i\Lambda_k X)\right\} + 2\pi i e^{i\Lambda_2 X}, \tag{21b}$$

where

$$\Phi(X) \equiv \sum_{k=1}^{3} A_k e^{i\Lambda_k X}\ln(i\Lambda_k X). \tag{21c}$$

Since $\chi(Z) \equiv -\gamma - \sum_{n=1}^{\infty}\frac{(-1)^n Z^n}{nn!}$ is an entire function, the source of singularity at $X = 0$ can only come from the *ln term* in the series, which we highlight by $\Phi(X)$ defined by (21c). This function can be written as

$$\Phi(X) = \sum_{k=1}^{3} A_k \ln(i\Lambda_k) e^{i\Lambda_k X} + \sum_{k=1}^{3} A_k\left(e^{i\Lambda_k X} - 1\right)\ln X + \ln X \underbrace{\sum_{k=1}^{3} A_k}_{0} = \sum_{k=1}^{3} A_k \ln(i\Lambda_k) e^{i\Lambda_k X} + \sum_{k=1}^{3} A_k\left(e^{i\Lambda_k X} - 1\right)\ln X \tag{22}$$

where we have used (17b). The first term of (22) is an entire function of X while the second term vanishes as $X \to 0^+$, so I is continuous at $X = 0$. Differentiating (22), we have

$$\Phi'(X) = i\sum_{k=1}^{3} A_k \Lambda_k \ln(i\Lambda_k)\, e^{i\Lambda_k X} + \sum_{k=1}^{3} A_k \left\{ \left(e^{i\Lambda_k X} - 1\right) \frac{1}{X} + (i\Lambda_k)\, e^{i\Lambda_k X} \ln X \right\} \tag{23a}$$

The first *two terms* of (23a), i.e.,

$$i\sum_{k=1}^{3} A_k \Lambda_k \ln(i\Lambda_k)\, e^{i\Lambda_k X} + \sum_{k=1}^{3} A_k \left(e^{i\Lambda_k X} - 1\right) \frac{1}{X} \tag{23b}$$

is analytic for all X (the 2nd term in (23b) has a removable singularity at the origin). The last term of (23a) is

$$i \ln X \sum_{k=1}^{3} A_k \Lambda_k e^{i\Lambda_k X} \to i \ln X \left[\underbrace{A_1 \Lambda_1}_{real} + \underbrace{A_2 \Lambda_2 + \overline{A}_2 \overline{\Lambda}_2}_{real} \right] \quad \text{as } X \to 0^+ \tag{24a}$$

A direct calculation using (16) and (17) show that $A_1\Lambda_1 + A_2\Lambda_2 + \overline{A}_2\overline{\Lambda}_2 = 0$, hence $\Phi'(X)$ is also continuous at $X = 0$; and by (21b), I'' is continuous at $X = 0$. In summary, we have completely determined the asymptotic behavior of the deformation at $X = 0$ by showing that

$$\Phi(X) = \sum_{k=1}^{3} A_k \ln(i\Lambda_k)\, e^{i\Lambda_k X} + \sum_{k=1}^{3} A_k \left(e^{i\Lambda_k X} - 1\right) \ln X \tag{24b}$$

$$\Phi'(X) = i\sum_{k=1}^{3} A_k \Lambda_k \ln(i\Lambda_k)\, e^{i\Lambda_k X} + \sum_{k=1}^{3} A_k \left(e^{i\Lambda_k X} - 1\right) \frac{1}{X} \tag{24c}$$

Therefore,

$$I(X) = I_1 + iI_2 = \frac{1}{2\pi} \left\{ \sum_{k=1}^{3} A_k e^{i\Lambda_k X} \chi(i\Lambda_k X) + 2\pi i A_2 e^{i\Lambda_2 X} - \Phi(X) \right\} \tag{25a}$$

$$= \frac{1}{2\pi} \left\{ \sum_{k=1}^{3} A_k e^{i\Lambda_k X} \chi(i\Lambda_k X) + 2\pi i A_2 e^{i\Lambda_2 X} - \sum_{k=1}^{3} A_k \ln(i\Lambda_k)\, e^{i\Lambda_k X} - \ln X \sum_{k=1}^{3} A_k \left(e^{i\Lambda_k X} - 1\right) \right\}$$

A simple calculation using (25a) shows that

$$I(X = 0, Y = 0) = \frac{1}{2\pi} \int_0^\infty C(\Lambda)\, d\Lambda = \frac{1}{2\pi} \left\{ A_1 \ln \left| \frac{\Lambda_2}{\Lambda_1} \right| - 2(\pi - Arg\,\Lambda_2)\, \mathrm{Im} A_2 \right\} \tag{25b}$$

The normalized surface displacement gradient profile for an incompressible substrate is shown in Fig. 3 for different κ. Fig. 3 shows that displacement is smooth function of position. As κ increases, there exist a region near the line load where the slope is approximately constant. For this case, bending is confined to a very small region near the line load; away from this region but at distances small in comparison with the elasto-capillary length, the surface kinks with an angle that satisfies the Neumann's triangle balance of forces.

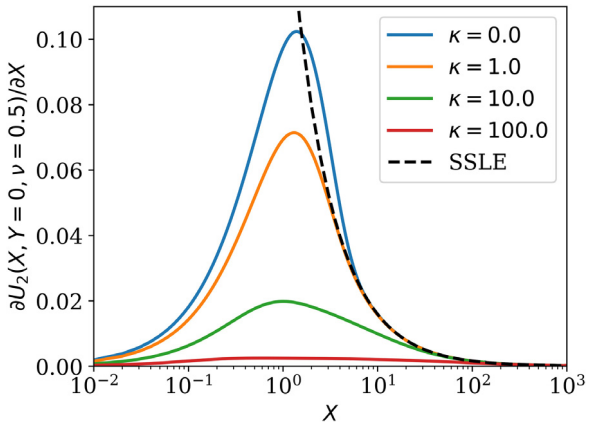

Fig. 3. The normalized surface displacement gradient of an incompressible substrate ($\beta = 1$)with different κ (solid lines), and the classic solution (dashed line). As κ increases, the slope near the line load is approximately constant; at distance large compares with the elasto-capillary and elasto-bending lengths the solution converges to the classic elasticity solution.

Finally, it can be easily shown that the displacement and stress fields at distance far from the line load are governed by the elasticity of the substrate, that is, for $|Z| \gg 1$, the stress and displacement gradients approach the classical solution by assuming small strain linear elasticity (SSLE), where these quantities decay as $1/|Z|$.

3.3. Stresses

Eqs. (13c–e) and the fact that I' is continuously differentiable at the origin implies that the *stresses and strains are continuously differentiable everywhere*. The maximum stress occurs at the origin, right underneath the line load. Eq. (13e) implies that the shear stress vanishes at the origin, so σ_{11}, σ_{22} are the principal stresses there. In addition, (13c, d) imply that $\sigma_{11}(x, y = 0) = \sigma_{22}(x, y = 0)$. This stress state deviates significantly from the classical elastic solution where the stresses have a $1/r$ singularity at the origin. Furthermore, the magnitude of the shear stress for this case depends on the direction. Specifically, it approaches infinity fastest as one approaches the origin along the rays $ArgZ = \pi/2 \pm \sin^{-1}\left(1/\sqrt{3}\right)$ (or 54.74° , 125.26° respectively). In contrast, the maximum shear stress occurs at some distance away from the line load, as will be shown below.

Denote the maximum of $|\sigma_{22}|$ by $\left|\sigma_{22}^{max}\right|$. According to (13c), it is

$$\left|\sigma_{22}^{max}\right| = 2\frac{|N|}{l_b} |I_1(Z = 0)| \tag{26}$$

where $I_1(Z = 0)$ is given by (25b). Note that the maximum of $\left|\Sigma_{22}^{max}\right|$ occurs at $\kappa = 0$ and is equal to $2/3\sqrt{3}$. Also, to compare with previous works, we also normalize the maximum stress $\left|\sigma_{22}^{max}\right|$ by $|N|/l_c$, and define this new normalized maximum stress by $\left|\Sigma_{22}^{max}\right|_c \equiv \left|\sigma_{22}^{max}\right| l_c/|N| = 2\kappa I_1(Z = 0)$. Fig. 4 shows that in the limit where surface stress dominates, the stress will be becomes unbounded, consistent with previous works [18].

To study the effect of Poisson's ratio on the normalized maximum stress $\left|\Sigma_{22}^{max}\right|$, we write $\kappa = [2(1-\upsilon)]^{2/3}\kappa^0$ where $\kappa^0 \equiv \frac{\sigma}{2\mu}/\sqrt[3]{\frac{D}{2\mu}}$ is independent of Poisson's ratio of the substrate. Fig. 5 shows that when κ^0 is small (surface bending dominates) $\left|\Sigma_{22}^{max}\right|$ is insensitive to the Poisson's ratio. However, for large κ^0 (surface tension dominates), $\left|\Sigma_{22}^{max}\right|$ is more sensitive to Poisson's ratio.

The normalized stress distribution Σ_{22} on the surface can be obtained using (13c) and (15) and is shown in Fig. 6 for different

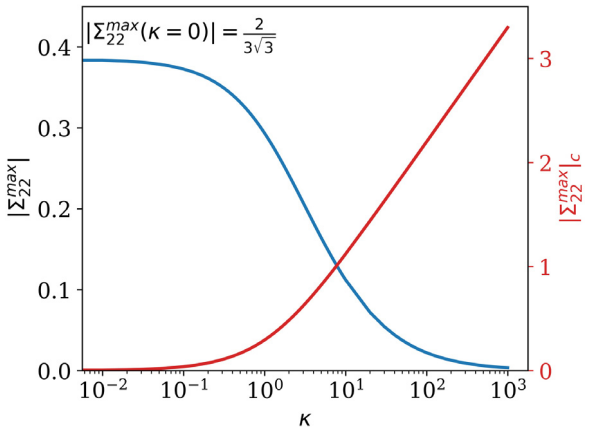

Fig. 4. Normalized maximum stress $\left|\Sigma_{22}^{max}\right|$ decreases as κ increases. In particular at $\kappa = 0$, the normalized maximum stress $\left|\Sigma_{22}^{max}\right|$ is bounded and equal to $2/\left(3\sqrt{3}\right)$. Normalized maximum stress $\left|\Sigma_{22}^{max}\right|_c$ increases as κ increases and indicates the unbounded behavior when surface stress dominates ($\kappa \to \infty$).

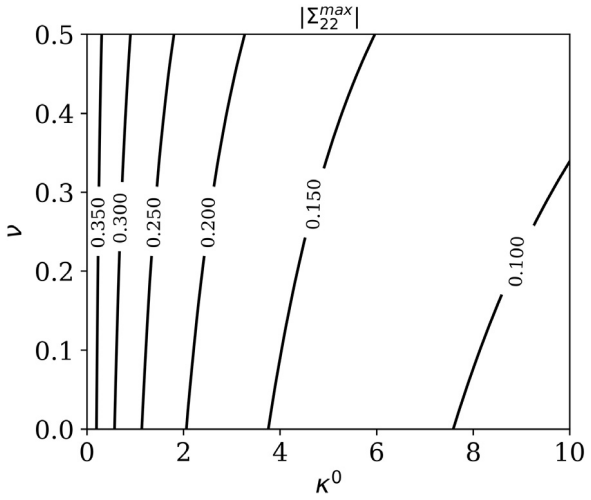

Fig. 5. Poisson ratio's effect on the normalized maximum stress $\left|\Sigma_{22}^{max}\right|$. $\left|\Sigma_{22}^{max}\right|$ is insensitive to the Poisson's ratio when κ^0 is small, and decreases distinctly as the Poisson's ratio decrease when κ^0 is large.

values of κ. The case of $\kappa = 0$ corresponds to a surface that has no resistance to stretching; for this case, all the applied load is supported by local shear force induced by the jump in moment.

We use (13c–e) and (21b) to compute all the stress components in the substrate. Contour plots of these stresses for $\kappa = 1$ are shown in Fig. 7a–c. The maximum value of the normalized shear stress $|\Sigma_{12}|$ denoted by $\left|\Sigma_{12}^{\max}\right|$ does not occur at the origin and locations of these maxima $(|Z_S|, ArgZ_S)$, as well as $\left|\Sigma_{12}^{\max}\right|$, are plotted against κ in Fig. 8. Note that $ArgZ_s \approx 42^0$, approximately independent of κ.

4. Discussion and summary

In this work we have examined in some detail what happens to the transmission of a line load on a half space if it is bounded by a surface that carries bending energy. Bending regularizes the solution, making surface displacements smooth everywhere, for example. The characteristic distance from the line force over which bending matters is given by the elasto-bending length. We return to the examples cited in the introduction to estimate the value

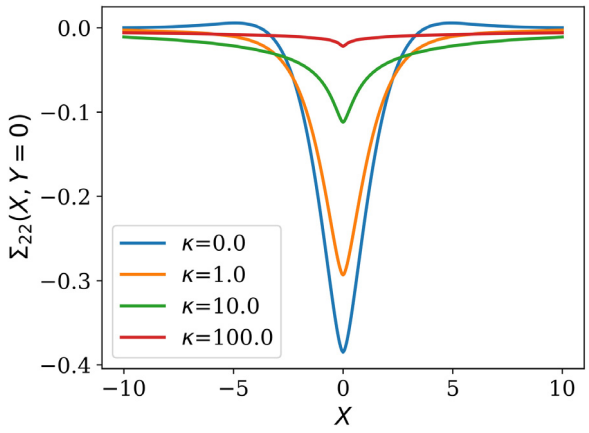

Fig. 6. Normalized stress distribution Σ_{22} on the surface. The stress fields are all smooth. As κ increases the normalized stress will decrease.

of the elasto-bending length. A typical value for bending modulus of a lipid bilayer at room temperature is about 20 k_BT, where k_B is the Boltzmann's constant and T the absolute temperature in Kelvin [30], and elastic modulus of a red blood cell is about 10 Pa [31]. Therefore, in this case, we expect a surface elasto-bending length to be about 200 nm. This length is much larger than the bilayer thickness (4–5 nm) implying that bending of the membrane is likely to balance a significant portion of any applied external load. For the second example in the introduction, a typical width of the silicaceous film on PDMS is 20 nm, and its modulus is about 2 GPa [32]; the modulus of PDMS is about 1 MPa. Thus, the elasto-bending length would be about 100 nm, much larger than the usual elasto-capillary length (∼20 nm).

In summary, we have presented an exact closed-form solution demonstrating how a normal line load is transmitted across a solid surface which carries both surface stress and surface bending. Our analyses have shown that surface bending completely regularizes the singularities in displacement and stress fields, which is not the case if we consider surface stress only. We found that the maximum stress and strains are insensitive to Poisson's ratio of the substrate when surface bending dominates, in contrast to the case where surface is dominated by surface stress.

Generally, if $l_c \gg l_b > 0$, one can expect to find three distinct regions. The one closest to the point of force application is smooth and dominated by bending. Its extent is given by the elasto-bending length. The farthest region is where the well-known small strain linear elastic solution applies; the displacements vary logarithmically with distance. Finally, there is an intermediate region with inner boundary given by the elasto-bending length and the outer one by the elasto-capillary length. In this region, surface stress dominates, the shape of the deformed surface is a straight line, the extension of which to the origin would meet in Neumann's triangle. Fig. 9 depicts this situation. If $l_c \ll l_b$, then there is no region where surface stress dominates, only one region where bending dominates and an outer region where we obtain the SSLE solution.

The vertical displacement in the SSLE solution diverges at the origin. It can approximately be regularized by invoking failure of continuum assumptions, but this would be at a molecular scale. Introduction of elastocapillarity changes the shape to a kink and, while reducing the singularity in stresses, does not eliminate them entirely. So, again, one needs to invoke some regularization at the molecular scale. The smoothness and complete regularization provided by the introduction of bending is of a different nature. The solution is now regularized over a length scale that is, as estimated above, much larger than molecular dimensions. That is, we may

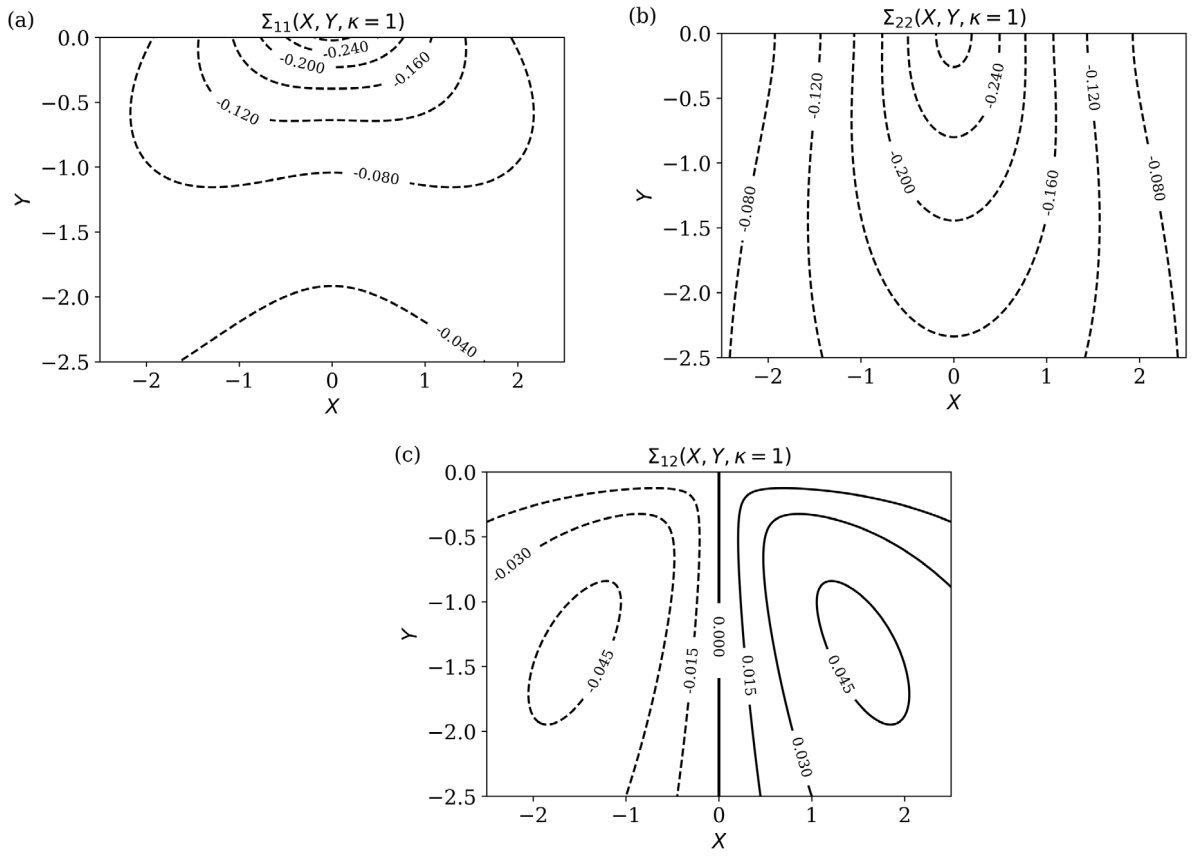

Fig. 7. Contour plots of normalized stresses for $\kappa = 1$ case. (a) $|\Sigma_{11}|$; (b) $|\Sigma_{22}|$; and (c) $|\Sigma_{12}|$.

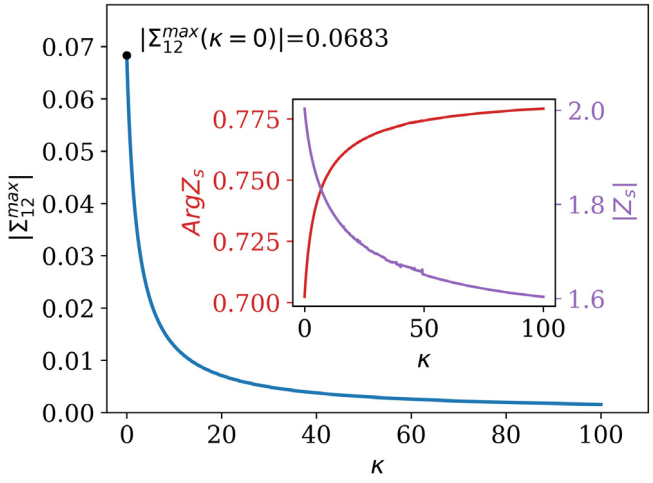

Fig. 8. Normalized maximum shear stress $|\Sigma_{12}^{max}|$ decreases as κ increases. At $\kappa = 0$, $|\Sigma_{12}^{max}|$ is bounded and gets its maximum value of 0.0683. The inset plot shows that as κ increases, the principle argument $ArgZ_s$ grows while $|Z_s|$ becomes shorter.

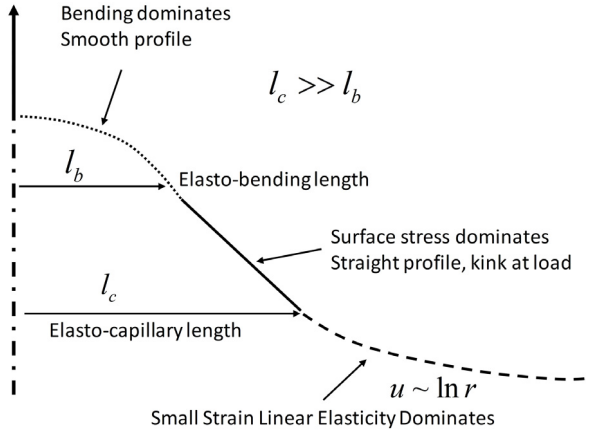

Fig. 9. Schematic drawing of the deformed surface of a soft body due to a line load. In general, we expect the surface to have three characteristic regions. In the region closest to the load, bending dominates, smoothen the surface and regularizing completely the displacement and stress fields. If the elasto-capillary length is significantly larger than the elasto-bending length, then for distance that lie between the two, we find a region where surface stresses dominate. The surface shape consists of straight lines that, if extended to the origin, would meet in Neumann's Triangle. Finally, sufficiently removed from the point of load application, the surfaces follow the SSLE solution, which decays logarithmically with distance.

invert this process and could view experimental determination of smoothness over large dimensions (compared to the molecular scale) as evidence of the presence of bending.

Although our model is based on small strain theory, our recent finite element simulations suggested that it should be valid for moderately large deformation [18]. Indeed, Wu et al. [18] shows that, for a surface with constant surface stress, the Neumann triangle of forces holds for $N/\sigma_0 < 1$ which corresponds to $\theta_k \approx 30^o$- a significant amount of deformation. Since surface bending further regularizes the local stress and strain fields, one would expect that the linearized solution presented here would be even more robust. However, our surface stress model does not account for the fact that surface stress can increase due to stretching [9,14]. Our calculation suggested that, as long as $l_b > l_c$, surface bending dominates surface stress; in this regime, surface stiffening due to

stretching should have little effect on our solution. In the other regime where $l_b < l_c$, our recent finite element simulations (Wu et al. [18]) showed that as long as $N/\sigma_0 < 1$, surface deformation for different surface stiffening elasticity is well approximated by the constant surface stress model. However, large deformation and surface stiffening comes into play when $N/\sigma_0 > 1$. More work needs to be done to clarify the effect of large deformation and the effect of surface shear.

Acknowledgments and funding source

All the authors acknowledge the support by the U.S. Department of Energy, Office of Basic Energy Sciences, Division of Materials Sciences and Engineering under Award DE-FG02-07ER46463.

Declarations of interest

None.

Submission declaration and verification

This work has not been published previously.

Ethics statement

This work does not involve human subjects or animals.

Data accessibility statement

This work does not have any experimental data.

Author agreement

All authors gave final approval for publications.

Appendix A. Supplementary data

Supplementary material related to this article can be found online at https://doi.org/10.1016/j.eml.2018.07.003.

References

[1] R.W. Style, A. Jagota, C.-Y. Hui, E.R. Dufresne, Elastocapillarity: Surface Tension and the mechanics of soft solids, Annu. Rev. Condens. Matter Phys. 8 (2017) 99–118. http://dx.doi.org/10.1146/annurev-conmatphys-031016-025326.

[2] R.C. Cammarata, Generalized surface thermodynamics with application to nucleation, Phil. Mag. 88 (2008) 927–948. http://dx.doi.org/10.1080/14786430802014654.

[3] R.C. Cammarata, K. Sieradzki, Surface and interface stresses, Annu. Rev. Mater. Sci. 24 (1994) 215–234. http://dx.doi.org/10.1146/annurev.ms.24.080194.001243.

[4] N. Nadermann, C.-Y. Hui, A. Jagota, Solid surface tension measured by a liquid drop under a solid film, Proc. Natl. Acad. Sci. 110 (2013) 10541–10545. http://dx.doi.org/10.1073/pnas.1304587110.

[5] R.W. Style, R. Boltyanskiy, Y. Che, J.S. Wettlaufer, L.A. Wilen, E.R. Dufresne, Universal deformation of soft substrates near a contact line and the direct measurement of solid surface stresses, Phys. Rev. Lett. 110 (2013) 066103. http://dx.doi.org/10.1103/PhysRevLett.110.066103.

[6] T. Liu, A. Jagota, C.-Y. Hui, Adhesive contact of a rigid circular cylinder to a soft elastic substrate? the role of surface tension, Soft Matter 11 (2015) 3844–3851. http://dx.doi.org/10.1039/C5SM00008D.

[7] R.W. Style, C. Hyland, R. Boltyanskiy, J.S. Wettlaufer, E.R. Dufresne, Surface tension and contact with soft elastic solids, Nature Commun. 4 (2013) 2728. http://dx.doi.org/10.1038/ncomms3728.

[8] Z. Cao, M.J. Stevens, A.V. Dobrynin, Adhesion and wetting of nanoparticles on soft surfaces, Macromolecules 47 (2014) 3203–3209. http://dx.doi.org/10.1021/ma500317q.

[9] M.E. Gurtin, A. Ian Murdoch, A continuum theory of elastic material surfaces, Arch. Ration. Mech. Anal. 57 (1975) 291–323. http://dx.doi.org/10.1007/BF00261375.

[10] R. Shuttleworth, The surface tension of solids, Proc. Phys. Soc. Sect. A 63 (1950) 444. http://dx.doi.org/10.1088/0370-1298/63/5/302.

[11] D.J. Steigmann, R.W. Ogden, Elastic surface—substrate interactions, Proc. R. Soc. Lond. Ser. Math. Phys. Eng. Sci. 455 (1999) 437. http://dx.doi.org/10.1098/rspa.1999.0320.

[12] D.J. Steigmann, Equilibrium of elastic lattice shells, J. Eng. Math. 109 (2018) 47–61. http://dx.doi.org/10.1007/s10665-017-9905-y.

[13] W. Helfrich, Elastic properties of lipid bilayers: Theory and possible experiments, Z. Naturforsch. C. 28 (2014) 693. http://dx.doi.org/10.1515/znc-1973-11-1209.

[14] K.E. Jensen, R.W. Style, Q. Xu, E.R. Dufresne, Strain-dependent solid surface stress and the stiffness of soft contacts, Phys. Rev. X 7 (2017) 041031. http://dx.doi.org/10.1103/PhysRevX.7.041031.

[15] H. Kusumaatmaja, Y. Li, R. Dimova, R. Lipowsky, Intrinsic contact angle of aqueous phases at membranes and vesicles, Phys. Rev. Lett. 103 (2009) 238103. http://dx.doi.org/10.1103/PhysRevLett.103.238103.

[16] A. Marchand, S. Das, J.H. Snoeijer, B. Andreotti, Contact angles on a soft solid: From Young's Law to Neumann's Law, Phys. Rev. Lett. 109 (2012) 236101. http://dx.doi.org/10.1103/PhysRevLett.109.236101.

[17] K.L. Johnson, Contact Mechanics, Cambridge University Press, Cambridge, 1985.

[18] H. Wu, Z. Liu, A. Jagota, C.-Y. Hui, Effect of large deformation and surface stiffening on the transmission of a line load on a neo-hookean half space, Soft Matter 14 (2018) 1847–1855. http://dx.doi.org/10.1039/C7SM02394D.

[19] C.-Y. Hui, A. Jagota, Deformation near a liquid contact line on an elastic substrate, Proc. R. Soc. Math. Phys. Eng. Sci. 470 (2014). http://dx.doi.org/10.1098/rspa.2014.0085. 20140085–20140085.

[20] A. Carre, J.-C. Gastel, M.E.R. Shanahan, Viscoelastic effects in the spreading of liquids, Nature 379 (1996) 432–434. http://dx.doi.org/10.1038/379432a0.

[21] L. Limat, Straight contact lines on a soft, ncompressible solid, Eur. Phys. J. E. 35 (2012) 134. http://dx.doi.org/10.1140/epje/i2012-12134-6.

[22] R.W. Style, E.R. Dufresne, Static wetting on deformable substrates, from liquids to soft solids, Soft Matter 8 (2012) 7177–7184. http://dx.doi.org/10.1039/C2SM25540E.

[23] J.T. Jenkins, Static equilibrium configurations of a model red blood cell, J. Math. Biol. 4 (1977) 149–169. http://dx.doi.org/10.1007/BF00275981.

[24] C.M. Stafford, C. Harrison, K.L. Beers, A. Karim, E.J. Amis, M.R. VanLandingham, H.-C. Kim, W. Volksen, R.D. Miller, E.E. Simonyi, A buckling-based metrology for measuring the elastic moduli of polymeric thin films, Nature Mater. 3 (2004) 545–550. http://dx.doi.org/10.1038/nmat1175.

[25] P.-C. Lin, S. Vajpayee, A. Jagota, C.-Y. Hui, S. Yang, Mechanically tunable dry adhesive from wrinkled elastomers, Soft Matter 4 (2008) 1830–1835. http://dx.doi.org/10.1039/B802848F.

[26] C. Py, P. Reverdy, L. Doppler, J. Bico, B. Roman, C.N. Baroud, Capillary origami: Spontaneous wrapping of a droplet with an elastic sheet, Phys. Rev. Lett. 98 (2007). http://dx.doi.org/10.1103/PhysRevLett.98.156103.

[27] J.D. Paulsen, V. Démery, C.D. Santangelo, T.P. Russell, B. Davidovitch, N. Menon, Optimal wrapping of liquid droplets with ultrathin sheets, Nature Mater. 14 (2015) 1206–1209. http://dx.doi.org/10.1038/nmat4397.

[28] K. Marguerre, Spannungsverteilung und wellenausbreitung in der kontinuierlich gestützten Platte, Ing.-Arch. 4 (1933) 332–353. http://dx.doi.org/10.1007/BF02081558.

[29] M. Abramowitz, I.A. Stegun, HandBook of Mathematical Functions: With Formulas, Graphs, and Mathematical Tables, Courier Corporation, 1964.

[30] D. Boal, D.H. Boal, Mechanics of the Cell, Cambridge University Press, 2012.

[31] T.W. Hoeber, R.M. Hochmuth, Measurement of red cell modulus of elasticity by in-vitro and model cell experiments, J. Basic Eng. 92 (1970) 604–609. http://dx.doi.org/10.1115/1.3425084.

[32] S. Béfahy, P. Lipnik, T. Pardoen, C. Nascimento, B. Patris, P. Bertrand, S. Yunus, Thickness and elastic modulus of plasma treated PDMS silica-like surface layer, Langmuir 26 (2010) 3372–3375. http://dx.doi.org/10.1021/la903154y.